JACS
JOURNAL OF THE AMERICAN CHEMICAL SOCIETY
pubs.acs.org/JACS
Article

Effect of Spatial Heterogeneity on the Unusual Uptake Behavior of Multivariate-Metal−Organic Frameworks

Soyeon Ko,[#] UnJin Ryu,[#] Hyunjin Park, Alejandro M. Fracaroli, WooYeon Moon, and Kyung Min Choi*

Cite This: https://doi.org/10.1021/jacs.2c12207
Read Online
ACCESS | Metrics & More | Article Recommendations | Supporting Information

ABSTRACT: The uniqueness of multivariate metal−organic frameworks (MTV-MOFs) has been widely explored to discover their unknown opportunities. While mesoscopic apportionments have been studied, macroscopic heterogeneity and its spatial effects remain unexplored in MTV-MOFs. In this study, we investigated the effect of macroscopic heterogeneity on MTV-MOFs on their uptake behaviors by comparing three types of MTV-MOFs having the functional groups in inner, outer, or entire parts of crystals. Their adsorption behavior for carbon dioxide (CO_2) and water (H_2O) brought out that functional groups located in the outer part of the crystals dominantly influence the sorption behavior of MTV-MOFs. These results are also visualized by observing iodine adsorption in the three types of MTV-MOFs using scanning transmission electron microscopy−electron energy loss spectroscopy. We believe that this finding provides new ways to decipher and design MTV-MOFs for their unusual properties.

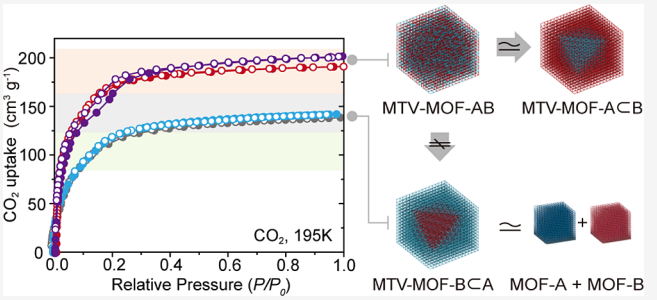

INTRODUCTION

Multivariate metal−organic frameworks (MTV-MOFs) introduce heterogeneity by incorporating multiple functional groups without changing the material's underlying topology. This heterogeneity leads to unusual adsorption properties that have not been observed in homogeneous MOFs having single functional groups.[1−4] The unique adsorption properties in MTV-MOFs have been deciphered by apportionments of multiple functional groups existing all over the crystals,[5−8] which is one of the key factors to discover unknown opportunities of MTV-MOFs. It was observed that different mesoscopic apportionment scenarios such as small cluster formation, random distribution, and well-mixed organic struts have an important impact on the sorption properties of MTV-MOFs.[5] Expanding the scope of this strategy, we hypothesized that controlling the spatial locality of the apportionment would influence the unique sorption behavior and unveil important factors contributing to MTV-MOFs.

In this study, we chose zirconium-based MOFs themed UiO-66 and two different organic struts considering the affinity differences with respect to polar adsorbates such as CO_2 and H_2O: 1,4-benzenedicarboxylate (denoted as BDC-H or simply A) and 2-amino-1,4-benzenedicarboxylate (denoted as BDC-NH_2 or simply B). Three types of materials were prepared to elucidate the decisive role of spatial locality in MTV-MOFs; (1) MTV-UiO-66-AB containing BDC-H (A) and BDC-NH_2 (B) linkers all over the crystals, as shown in Scheme 1a, (2) MTV-UiO-66-A ⊂ B having a BDC-NH_2 linker outer part and a BDC-H linker inner part of its crystals, as shown in Scheme 1b, and (3) MTV-UiO-66-B ⊂ A having a BDC-H linker outer

Scheme 1. Schematic Diagram for MTV-MOF with Two Distinct Linkers of BDC-H (A) and BDC-NH_2 (B): (a) MTV-UiO-66-AB, (b) MTV-UiO-66-A ⊂ B, and (c) MTV-UiO-66-B ⊂ A

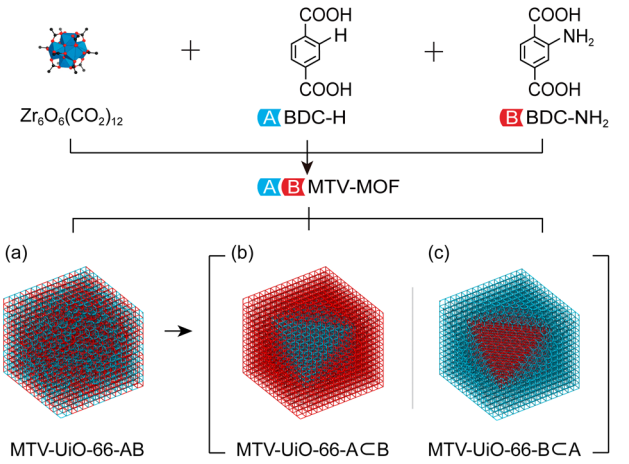

Received: November 17, 2022

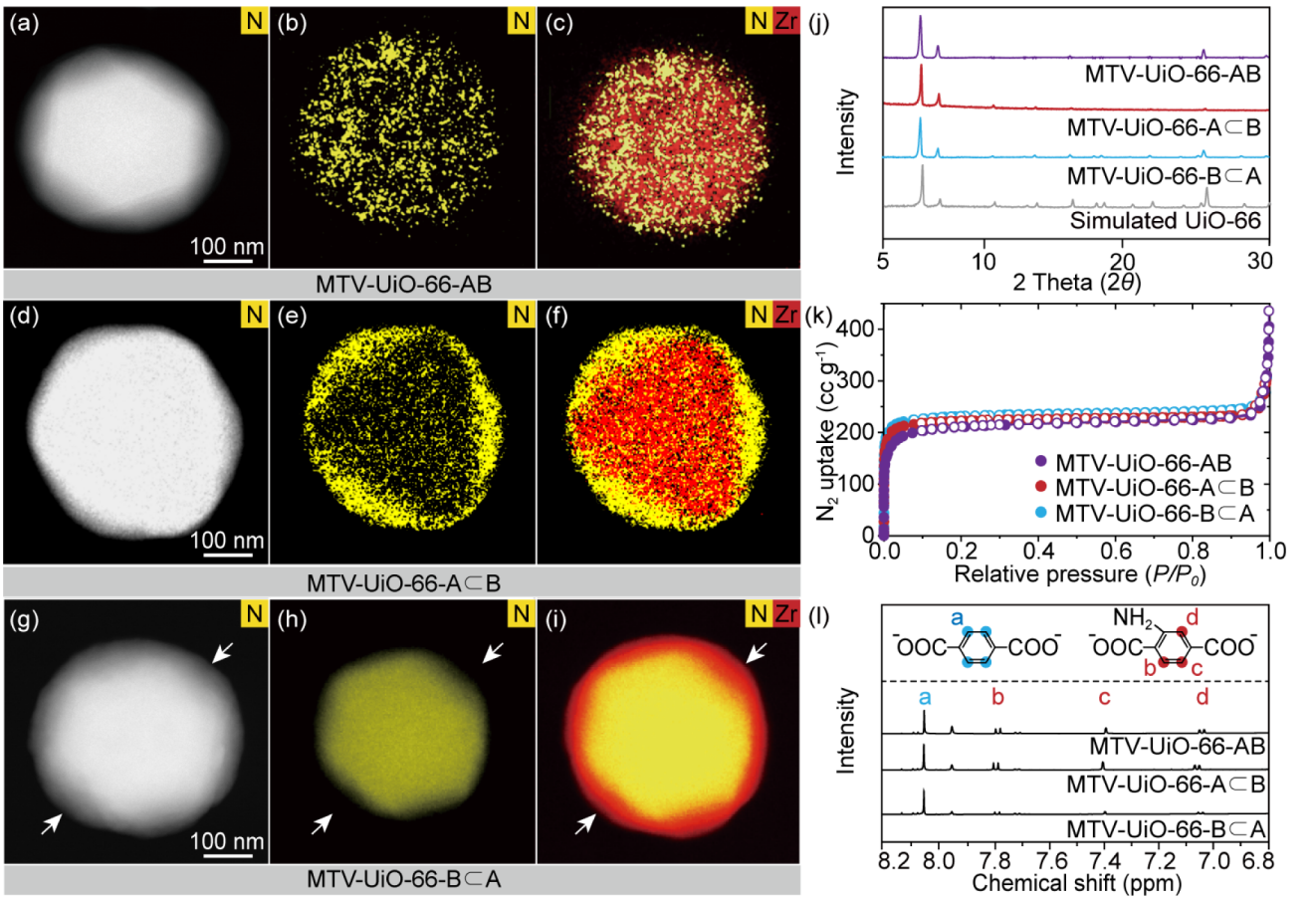

Figure 1. Characterization of spatially localized MTV-MOF crystals. (a–i) STEM images (left) and EELS-derived maps of nitrogen (center) and nitrogen/zirconium (right) for MTV-MOFs. (a–c) MTV-UiO-66-AB (d–f) MTV-UiO-66-A ⊂ B (g–i) MTV-UiO-66-B ⊂ A. (j) PXRD patterns, (k) N_2 sorption isotherms at 77 K, and (l) digested-^{1}H NMR spectra of MTV-MOFs.

part and a BDC-NH_2 linker inner part of its crystals, as shown in Scheme 1c. Furthermore, three types of homogeneous MOFs, UiO-66-A, UiO-66-B, and mechanical mixtures of UiO-66-A and UiO-66-B (mix-UiO-66-AB), were also prepared for comparison. All the MOFs prepared were tested for CO_2 uptake at 195 K. It was observed that the sorption behavior of MTV-UiO-66-AB was similar to that of UiO-66-B regardless of the ratio between BDC-H and BDC-NH_2. Interestingly, the CO_2 uptake behavior of MTV-UiO-66-A ⊂ B resembled that of UiO-66-B while the isotherm for MTV-UiO-66-B ⊂ A resembled that of the physical mixture of UiO-66-A and UiO-66-B. In the case of H_2O uptake measured at 298 K, it was found that the uptake behavior of MTV-MOFs showed a similar trend to that of CO_2. These pieces of evidence of CO_2 and H_2O uptake support that the sorption behavior of MTV-UiO-66-AB was strongly affected by the specific functionality present in the outer part of its crystal. These findings were also supported by visualization of iodine sorption using scanning transmission electron microscopy–electron energy loss spectroscopy (STEM–EELS).

In previous work, MTV-MOFs were studied to improve the selectivity and adsorption performance depending on their number, kind, and ratio of functional linkers.[9−11] Herein, this study focuses on the spatial location of functionality in MTV-MOFs and its effect on the unique sorption properties derived therefrom. Other studies have synthesized core/shell-type MOFs using different combinations of functionalities and then showed the properties derived from the structure.[12−15] However, our study adopts the core/shell type to decipher the unique sorption properties of MTV-MOFs and provides a new way to facilitate the spatially localized heterogeneities in MTV-MOFs, contributing unexpected properties.

RESULTS AND DISCUSSION

UiO-66 was selected as the basal structure to make MTV-MOFs because it has strong bonding between the organic linkers and the zirconium clusters maintaining its structure after the gas uptake process and even under accelerated electrons in TEM to observe the spatial locality of functionalities. We also choose BDC-NH_2 and BDC-H as the target functional linkers because they have different interactions with polar adsorbents and clearly demonstrate their effect depending on their spatial location in the MTV-MOF. We prepared 6 types of UiO-66 s to decipher the distinct adsorption behavior of MTV-MOF-AB (Scheme S1); three MTV-MOFs (MTV-UiO-66-AB, MTV-UiO-66-A ⊂ B, and MTV-UiO-66-B ⊂ A); and three homogeneous MOFs (UiO-66-A, UiO-66-B, and mix-UiO-66-AB). MTV-UiO-66-A ⊂ B and MTV-UiO-66-B ⊂ A were synthesized by the nanoparticle-mediated nucleation method (Figure S1).[16] UiO-66-A and UiO-66-B were synthesized from BDC-H and BDC-NH_2, respectively, in DMF containing dissolved $ZrCl_4$ at 120 °C. Pt nanoparticles (Pt NPs) were subsequently attached on their external surfaces inducing seed growth for outer MOF layers.[17] The outer MOF layers were formed in the synthetic solution having dispersed UiO-66-A and UiO-66-B particles to

https://doi.org/10.1021/jacs.2c12207
J. Am. Chem. Soc. XXXX, XXX, XXX−XXX

give MTV-UiO-66-A ⊂ B and MTV-UiO-66-B ⊂ A, respectively. When the UiO-66-A expanded to MTV-UiO-66-A ⊂ B, the color turned yellow from white, while the yellow color of UiO-66-B faded out as it became MTV-UiO-66-B ⊂ A. MTV-UiO-66-AB was prepared by mixing the two linkers of BDC-H and BDC-NH_2 in a preparation solution. The mix-UiO-66-AB was prepared by physically mixing UiO-66-A and UiO-66-B particles. All samples were washed using DMF and MeOH and dried in vacuo overnight. The products were characterized using scanning electron microscopy (SEM), STEM, EELS, powder X-ray diffraction (PXRD), N_2 adsorption, and nuclear magnetic resonance (NMR) spectroscopy. These techniques indicate the morphology, elemental distribution and ratio of functional groups, crystallinity, and porosity of samples. The SEM images showed that all types of MOF samples had a uniform octahedral shape of UiO-66 (Figure S2). The particles of MTV-UiO-66-A ⊂ B and MTV-UiO-66-B ⊂ A showed 450 and 400 nm diameter which were enlarged from UiO-66-A (300 nm) and UiO-66-B (350 nm), respectively. The EELS mapping showed the positions of the constituents in MTV-MOFs, while the STEM images showed their sizes and morphologies (Figure 1a–i). Zirconium, which constitutes the metal oxide cluster of UiO-66, was enriched throughout the whole crystals. The locations of NH_2-functional groups in MTV-MOFs were determined by the locations of nitrogen. MTV-UiO-66-AB showed evenly distributed NH_2-functional groups over the whole crystal, as shown in Figure 1b,c. In contrast, the NH_2-functional groups were clearly concentrated in the outer layers of MTV-UiO-66-A ⊂ B with a thickness of 150 nm (Figure 1e,f). In the case of MTV-UiO-66-B ⊂ A, an outer layer of 50 nm thickness having H-functional groups was formed around UiO-66-B (Figure 1h,i). These results confirmed that the locations of the NH_2-functional groups were partitioned and that they were consistent with the change in the size of the MOF crystals, as shown in the SEM images (Figure S2). As shown in Figures S3–S8, the EELS images indicated the presence or absence of NH_2-functional groups in homogeneous MOFs. The entire crystal of UiO-66-B consisted of NH_2-functional groups, which was not the case for UiO-66-A crystals. This was also evident in mix-UiO-66-AB, where UiO-66-A and UiO-66-B were physically mixed. The volumetric contents percentage of the inner and outer parts of the MTV-MOFs were back-calculated, as shown in Table S1. Fourier transform infrared (FT-IR) spectra were also collected to find out the presence of NH_2-functional groups in MTV-MOFs, UiO-66-B, and mix-UiO-66-AB (Figure S9).

The powder X-ray diffraction (PXRD) patterns of the MTV-MOFs showed sharp diffraction lines that are evidence of high crystallinity, and the coincidence of the diffraction lines matched with simulated UiO-66 patterns that clearly indicate the preservation of the UiO-66 structure regardless of the functional localization in the crystals (Figures 1j and S10). The permanent porosities of MTV-MOFs were confirmed by measuring the N_2 adsorption that showed type-I isotherms similar to those of UiO-66 (Figures 1k and S11). The MTV-MOFs had similar Langmuir surface areas with intermediate values between UiO-66-A and UiO-66-B (Table S2). The digested-^{1}H NMR measurements were performed to analyze the presence and ratio of BDC-H and BDC-NH_2 linkers in MTV-MOFs. The samples were prepared by adding strong acid in DMSO-d_6 to disconnect the linkers and metal oxide clusters of MTV-MOFs. Their ^{1}H NMR spectra are shown in Figures 1l and S12–S17. The spectra of MTV-UiO-66-AB, MTV-UiO-66-A ⊂ B, and MTV-UiO-66-B ⊂ A contained peaks at (a) 8.05 ppm and (b–d) 7.8, 7.4, and 7.05 ppm, corresponding to BDC-H and BDC-NH_2. The integration of these peaks revealed the ratio of BDC-H and BDC-NH_2 in all MOFs as noted in Table S3, which indicates that all MTV-MOFs have a similar ratio of 1:2 for BDC-H and BDC-NH_2. This value corresponded to the ratio back-counted from the volume fraction of the inner and outer parts of the MTV-MOFs in EELS mapping images (Table S1). Based on the similar ratio of BDC-H and BDC-NH_2 in all the MTV-MOFs, we can solely compare the impacts of spatially localized NH_2-functional groups in MTV-MOFs on their unique gas sorption properties.

We measured the CO_2 uptake properties to analyze the unusual sorption behavior of MTV-MOFs. CO_2 was selected as the adsorbate because it covalently bonds with the primary amine, which can improve the CO_2 uptake ability in the MTV-MOF system.[18−20] We examined the CO_2 sorption of MTV-MOFs and homogeneous MOFs at 195 K. All the samples were activated by being evacuated at 120 °C for 24 h in a vacuum before measurements. As shown in Figure 2a, UiO-66-

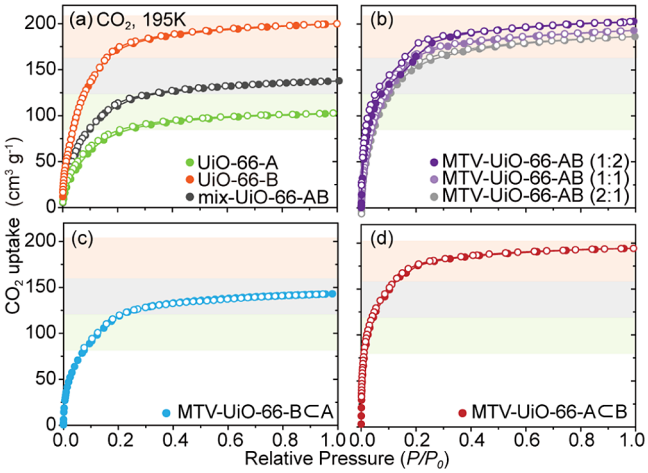

Figure 2. CO_2 sorption isotherm of (a) UiO-66-A, UiO-66-B, and mix-UiO-66-AB, (b) MTV-UiO-66-AB (1:2), MTV-UiO-66-AB (1:1), MTV-UiO-66-AB (2:1), (c) MTV-UiO-66-B ⊂ A, and (d) MTV-UiO-66-A ⊂ B. *MTV-UiO-66-AB (BDC-H/BDC-NH_2) were prepared by different ratios of BDC-H and BDC-NH_2 linkers.

B, which was entirely composed of NH_2-functional groups, showed higher total uptake than UiO-66-A. The result is due to the strong interaction between the NH_2-groups and CO_2 and is similar to the results of previous studies.[21−27] In the case of mix-UiO-66-AB, the total uptake was intermediate to those of UiO-66-A and UiO-66-B. Although MTV-UiO-66-AB contained a similar amount of NH_2-groups as mix-UiO-66-AB, its uptake behavior was similar to that of UiO-66-B. We also prepared multiple MTV-UiO-66-AB samples having different amine ratios, which were denoted as MTV-UiO-66-AB (*X*:*Y*), where *X* and *Y* are the ratios of BDC-H and BDC-NH_2, respectively. MTV-UiO-66-AB(1:2), MTV-UiO-66-AB(1:1), MTV-UiO-66-AB(2:1), MTV-UiO-66-AB(9:1), and MTV-UiO-66-AB(33:1) have the BDC-NH_2 content of 68.8, 46.7, 32.6, 9.9, and 2.9%, respectively (Table S3). Interestingly, the MTV-UiO-66-AB (*X*:*Y*) samples with a BDC-NH_2 content higher than 2.9% showed a similar uptake behavior and are also

https://doi.org/10.1021/jacs.2c12207
J. Am. Chem. Soc. XXXX, XXX, XXX−XXX

comparable to that of UiO-66-B (Figures 2b and S18). These results indicate that the CO_2 uptake is similar regardless of the ratio when functional groups of more than a certain number exist to facilitate the MTV-system. Therefore, we considered that the spatial location of NH_2-functional groups might be an important factor for determining the unusual sorption behavior of MTV-MOFs and tested the CO_2 uptake behaviors of MTV-UiO-66-A ⊂ B and MTV-UiO-66-B ⊂ A. We found that the isotherm of MTV-UiO-66-A ⊂ B was similar to that of UiO-66-B and all of the MTV-UiO-66-AB(X:Y) samples regardless of the ratio of NH_2-functional groups. On the other hand, the isotherm of MTV-UiO-66-B ⊂ A was similar to that of the physical mixture of UiO-66-A and UiO-66-B (mix-UiO-66-AB).

Based on the isotherms shown in Figure 2, we classified each of the MOFs tested into two groups: one containing NH_2-functional groups at the outer part [MTV-UiO-66-A ⊂ B, UiO-66-B, and MTV-UiO-66-AB(X:Y)] and the other without NH_2-functional groups at the outer part (MTV-UiO-66-B ⊂ A and UiO-66-A). The MOFs containing NH_2-functional groups at the outer part of the crystal showed similar CO_2 uptake behaviors whereas other samples showed the uptake behaviors that originated solely from the amount of BDC-H and BDC-NH_2 like the physical mixture (mix-UiO-66-AB). These results indicate that highly interactive functional groups present in the outer part dominantly influence the uptake behavior of the entire crystal, whereas those present in the inner part just contribute as much as its ratio. Considering that highly interactive functional groups spatially exist throughout the MTV-MOF crystals, the unique uptake behavior of MTV-MOF originates from the "outer part" rather than the "inner part".

The origin of the uniqueness was further investigated by comparing the adsorption behaviors in low relative pressure, which is presented in the logarithm scale in Figure S19. This graph focuses more on monolayer and multilayer adsorption of CO_2 in the samples. The first slope in the initial sorption stage presented a monolayer adsorption behavior and the second slope in the following stage presented a multilayer adsorption behavior in the pores of the samples. The amount of monolayer adsorption in MTV-UiO-66-A ⊂ B (48.6 cc g^{-1} at P/P_0 = 0.004) was much higher than MTV-UiO-66-AB (29.5 cc g^{-1} at P/P_0 = 0.006), UiO-66-B (29.2 cc g^{-1} at P/P_0 = 0.004), MTV-UiO-66-B ⊂ A (27.0 cc g^{-1} at P/P_0 = 0.005), UiO-66-A (9.6 cc g^{-1} at P/P_0 = 0.003), and mix-UiO-66-AB (9.4 cc g^{-1} at P/P_0 = 0.003). Moreover, the transition pressures from monolayer to multilayer adsorption in MTV-UiO-66-A ⊂ B (P/P_0 = 0.004) and MTV-UiO-66-AB (P/P_0 = 0.007) were much lower than those in MTV-UiO-66-B ⊂ A (P/P_0 = 0.02), UiO-66-A (P/P_0 = 0.04), UiO-66-B (P/P_0 = 0.02), and mix-UiO-66-AB (P/P_0 = 0.03). We speculate that these behaviors are originated by the sequential interrelation between the pore with a highly affinitive $-NH_2$ group (-B) and the pore with open space (-A). In the case of MTV-UiO-66-AB and MTV-UiO-66-A ⊂ B, the CO_2 molecules traveling into the samples would have high possibility to interact first with the $-NH_2$ group and then move into the open space. This enables a larger amount of monolayer adsorption and lower pressure transition to multilayer adsorption than other samples including homogeneous MOFs and MTV-UiO-66-B ⊂ A. We believe that this is the case of the communication sequence for the guest molecules coming into MTV-MOF samples.

We examined the H_2O uptake properties to confirm the dominant influence of functional groups in the outer part of the MTV-MOFs. Because the NH_2-functional groups influence the affinity with H_2O in MOFs, we tested H_2O uptake of the MTV-MOFs and homogeneous MOFs at 298 K under relative atmospheric pressure. All the samples were activated by evacuating at 120 °C for 24 h before measurements. Figure 3a shows a comparison of the isotherms for homogeneous MOFs. In contrast to the CO_2 isotherms at 195 K, UiO-66-B (411.3 cm^3g^{-1}) showed lower total uptake than UiO-66-A (517.7 cm^3g^{-1}) at P/P_0 = 0.95. This is because the presence of NH_2-groups make the pore smaller, decreasing the total water uptake rather than increasing affinity at room temperature.[28−31] However, the increased affinity makes H_2O uptake start at a lower relative pressure than UiO-66-A (Figure 3a). Figure 3b shows that MTV-MOF-AB(X:Y) had a similar total uptake in all amine ratios and their isotherms were similar to those of MOF-B, which is consistent with the CO_2 isotherm results (Figure 2b). MTV-UiO-66-B ⊂ A and MTV-UiO-66-A ⊂ B were tested to investigate the spatial effect of the NH_2-functional groups in or out of MTV-MOF particles on the H_2O adsorption capacity (Figure 3c,d) as investigated in CO_2 uptake analysis (Figure 2c,d). The total uptake and adsorption isotherm of MTV-UiO-66-B ⊂ A resembled those of UiO-66-A (Figure 3c). Similarly, MTV-UiO-66-A ⊂ B showed a correlative isotherm to those of MTV-UiO-66-AB(X:Y) and UiO-66-B (Figure 3d). This indicates that the uptake behavior of the outer part overwhelms that of the whole crystal of MTV-MOF.

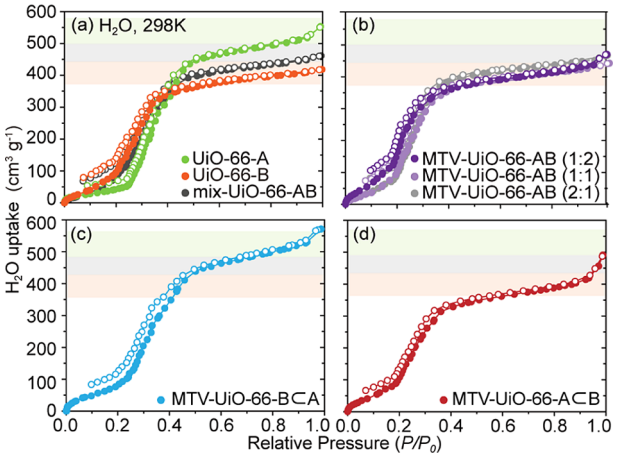

Figure 3. H_2O sorption isotherm of (a) UiO-66-A, UiO-66-B, and mix-UiO-66-AB, (b) MTV-UiO-66-AB (1:2), MTV-UiO-66-AB (1:1), MTV-UiO-66-AB (2:1), (c) MTV-UiO-66-B ⊂ A, and (d) MTV-UiO-66-A ⊂ B. *MTV-UiO-66-AB (BDC-H/BDC-NH_2) were prepared by different ratios of BDC-H and BDC-NH_2 linkers.

The effect of polarity on these usual uptake behaviors of MTV-MOFs was investigated by comparing the isotherms of CO_2 and N_2 at their boiling temperature (Figures 2 and S11) and the isotherms of H_2O and CO_2 at room temperature (298 K) (Figures 3 and S20). These comparisons showed that the unusual behaviors of MTV-MOFs were observed when the absorbate had sufficient interaction with functional groups at a given temperature. Therefore, the results make clear that spatial heterogeneity combined with the intermolecular interaction with functional groups highly effect on the unusual uptake behaviors of MTV-MOFs.

https://doi.org/10.1021/jacs.2c12207
J. Am. Chem. Soc. XXXX, XXX, XXX−XXX

The finding, that the uptake in the outer part affects the inner part in MTV-MOFs, was intuitively demonstrated by using the iodine sorption method. By exposing MTV-MOF particles to iodine, its vapor diffused into the MTV-MOFs can be visualized by elemental mapping images obtained in STEM−EELS measurements. As iodine has a high atomic number of 53, its presence is readily detected by STEM measurements.[32−35] Samples were prepared by placing each MOF sample on a separate TEM grid followed by being exposed to iodine for 2 days at room temperature in sealed vials to sufficiently diffuse the iodine vapor into the MOF crystals. The position of BDC-NH_2 was indicated by the yellow color in the nitrogen mapping images while the boundaries of the entire crystal are indicated by arrows in Figure 4a−c. The

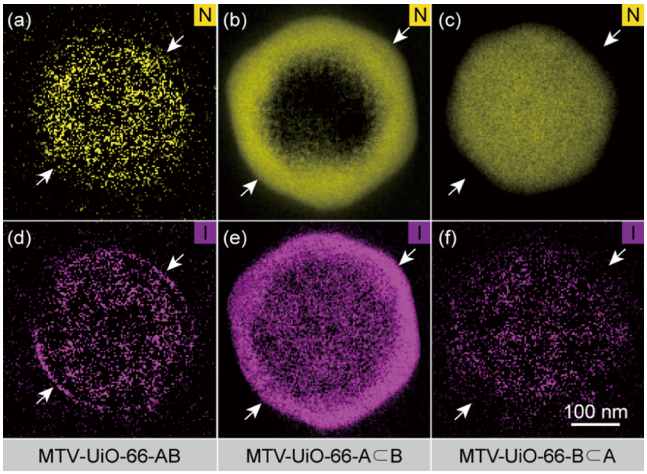

Figure 4. EELS elemental mapping images of nitrogen (top) and iodine (bottom) for spatial localized MTV-MOFs. (a,d) MTV-UiO-66-AB, (b,e) MTV-UiO-66-A ⊂ B, and (c,f) MTV-UiO-66-B ⊂ A.

iodine mapping images in Figure 4d−f indicate the presence of iodine by purple color. Because the NH_2-functional groups have polar hydrophilic interactions, iodine tends to be observed intensively in the NH_2-rich areas, as shown in Figure 4d−f.[36−39] In the case of MTV-UiO-66-AB, iodine was diffused throughout the crystal according to the distribution of the NH_2-functional groups (Figure 4d). Interestingly, MTV-UiO-66-A ⊂ B exhibited highly intensive iodine signals in the inner and outer parts of the crystal (Figure 4e). Because of the presence of the NH_2-functional groups in the outer part, the purple coloration of the outer part was more intense than that of the inner part. In contrast, iodine adsorbed by MTV-UiO-66-B ⊂ A majorly remains in the inner part, not in the outer part (Figure 4f). It should be noted that the intercomparison between different images for different samples is not allowed as each image has different brightness and contrast. Comparing the relative intensity of purple coloration in the pore with open space (-A) versus that in the pore with $-NH_2$ group (-B) in each sample, MTV-UiO-66-A ⊂ B has a higher intensity than MTV-UiO-66-B ⊂ A (Figure 4e,f). These results visualize that the uptake behavior of the outer part with the -NH_2 group (-B) affects that of the inner part with open space (-A) of the crystal in MTV-MOF. Therefore, we believe that the unique behavior of MTV-UiO-66-AB is influenced more strongly by the presence of the NH_2-functional groups in the "outer part" rather than the "inner part" of the crystal.

CONCLUSIONS

In this study, the unique adsorption properties of MTV-MOF were analyzed by implementing the spatial localization of functional groups in MTV-UiO-66-AB. Specifically, the locality was investigated by synthesizing MTV-UiO-66-A ⊂ B and MTV-UiO-66-B ⊂ A crystals having NH_2-functionalities in the outer and inner parts of the crystals, respectively. We tested the sorption properties of MTV-UiO-66-AB, MTV-UiO-66-A ⊂ B, and MTV-UiO-66-B ⊂ A using two adsorbates (CO_2 and H_2O) and eventually found that the uptake behavior in the outer part strongly influences that of the whole crystal in MTV-MOFs. Furthermore, this finding was also visualized using iodine adsorption and STEM-EELS observation. Considering these results, we propose to focus on the localization of functional heterogeneity in MTV-MOFs to explore their unique uptake behaviors.

ASSOCIATED CONTENT

Supporting Information

The Supporting Information is available free of charge at https://pubs.acs.org/doi/10.1021/jacs.2c12207.

Detailed experimental and experimental methods; additional SEM images; STEM-EELS images; FT-IR spectra; PXRD; N_2 adsorption; and NMR spectroscopy (PDF)

AUTHOR INFORMATION

Corresponding Author

Kyung Min Choi − *Department of Chemical and Biological Engineering and Muscle Physiome Research Center, Sookmyung Women's University, Seoul 04310, Republic of Korea;* orcid.org/0000-0001-7181-902X; Email: kmchoi@sookmyung.ac.kr

Authors

Soyeon Ko − *Department of Chemical and Biological Engineering, Sookmyung Women's University, Seoul 04310, Republic of Korea;* Present Address: Chemical Engineering, School for Engineering of Matter, Transport, and Energy, Arizona State University, Tempe, Arizona, 85281, United States (S.K.)

UnJin Ryu − *Industry Collaboration Center, Sookmyung Women's University, Seoul 04310, Republic of Korea;* Present Address: School of Chemical & Biomolecular Engineering, Georgia Institute of Technology, 311 Ferst Dr., Atlanta, Georgia 30332-0100, United States (U.R.); orcid.org/0000-0002-4854-3587

Hyunjin Park − *National Institute for Nanomaterials Technology, Pohang University of Science & Technology (POSTECH), Pohang 37673, Republic of Korea*

Alejandro M. Fracaroli − *Instituto de Investigaciones en Físico-química de Córdoba, INFIQC-CONICET, Facultad de Ciencias Químicas, Departamento de Química Orgánica, Universidad Nacional de Córdoba, Ciudad Universitaria, Córdoba X5000HUA, Argentina;* orcid.org/0000-0003-3016-6813

WooYeon Moon − *Department of Chemical and Biological Engineering, Sookmyung Women's University, Seoul 04310, Republic of Korea*

Complete contact information is available at: https://pubs.acs.org/10.1021/jacs.2c12207

Author Contributions

[#]S.K. and U.R. contributed equally to this paper.

Funding

This research was supported by the National Research Foundation of Korea (NRF) funded by the Ministry of Education (No. 2022R1A2B5B01001826 and 2022R1A5A2021216).

Notes

The authors declare no competing financial interest.

■ ACKNOWLEDGMENTS

The authors thank H.P. (POSTECH) for assistance with STEM-EELS measurements.

■ REFERENCES

(1) Zhang, Y. B.; Furukawa, H.; Ko, N.; Nie, W.; Park, H. J.; Okajima, S.; Cordova, K. E.; Deng, H.; Kim, J.; Yaghi, O. M. Introduction of Functionality, Selection of Topology, and Enhancement of Gas Adsorption in Multivariate Metal−Organic Framework-177. *J. Am. Chem. Soc.* **2015**, *137*, 2641−2650.

(2) Helal, A.; Yamani, Z. H.; Cordova, K. E.; Yaghi, O. M. Multivariate Metal-Organic Frameworks. *Natl. Sci. Rev.* **2017**, *4*, 296−298.

(3) Fan, W.; Yuan, S.; Wang, W.; Feng, L.; Liu, X.; Zhang, X.; Wang, X.; Kang, Z.; Dai, F.; Yuan, D.; Sun, D.; Zhou, H. C. Optimizing Multivariate Metal-Organic Frameworks for Efficient C_2H_2/CO_2 Separation. *J. Am. Chem. Soc.* **2020**, *142*, 8728−8737.

(4) Mon, M.; Bruno, R.; Tiburcio, E.; Viciano-Chumillas, M.; Kalinke, L. H. G.; Ferrando-Soria, J.; Armentano, D.; Pardo, E. Multivariate Metal-Organic Frameworks for the Simultaneous Capture of Organic and Inorganic Contaminants from Water. *J. Am. Chem. Soc.* **2019**, *141*, 13601−13609.

(5) Dong, Z.; Sun, Y.; Chu, J.; Zhang, X.; Deng, H. Multivariate Metal-Organic Frameworks for Dialing-in the Binding and Programming the Release of Drug Molecules. *J. Am. Chem. Soc.* **2017**, *139*, 14209−14216.

(6) Kong, X.; Deng, H.; Yan, F.; Kim, J.; Swisher, J. A.; Smit, B.; Yaghi, O. M.; Reimer, J. A. Mapping of Functional Groups in Metal-Organic Frameworks. *Science* **2013**, *341*, 882−885.

(7) Ji, Z.; Li, T.; Yaghi, O. M. Sequencing of Metals in Multivariate Metal-Organic Frameworks. *Science* **2020**, *369*, 674−680.

(8) Liu, Q.; Cong, H.; Deng, H. Deciphering the Spatial Arrangement of Metals and Correlation to Reactivity in Multivariate Metal−Organic Frameworks. *J. Am. Chem. Soc.* **2016**, *138*, 13822−13825.

(9) Feng, L.; Wang, K. Y.; Lv, X. L.; Powell, J. A.; Yan, T. H.; Willman, J.; Zhou, H. C. Imprinted Apportionment of Functional Groups in Multivariate Metal-Organic Frameworks. *J. Am. Chem. Soc.* **2019**, *141*, 14524−14529.

(10) Deng, H.; Doonan, C. J.; Furukawa, H.; Ferreira, R. B.; Towne, J.; Knobler, C. B.; Wang, B.; Yaghi, O. M. Multiple Functional Groups of Varying Ratios in Metal-Organic Frameworks. *Science* **2010**, *327*, 846−850.

(11) Osborn Popp, T. M.; Plantz, A. Z.; Yaghi, O. M.; Reimer, J. A. Precise Control of Molecular Self-Diffusion in Isoreticular and Multivariate Metal-Organic Frameworks. *ChemPhysChem* **2020**, *21*, 32−35.

(12) Xia, Q.; Li, Z.; Tan, C.; Liu, Y.; Gong, W.; Cui, Y. Multivariate Metal−Organic Frameworks as Multifunctional Heterogeneous Asymmetric Catalysts for Sequential Reactions. *J. Am. Chem. Soc.* **2017**, *139*, 8259−8266.

(13) He, Y.; Sun, M.; Zhao, Q.; Shang, J.; Tian, Y.; Xiao, P.; Gu, Q.; Li, L.; Webley, P. A. Effective Gas Separation Performance Enhancement Obtained by Constructing Polymorphous Core−Shell Metal−Organic Frameworks. *ACS Appl. Mater. Interfaces* **2019**, *11*, 30234−30239.

(14) Feng, L.; Wang, K. Y.; Day, G. S.; Zhou, H. C. The Chemistry of Multi-Component and Hierarchical Framework Compounds. *Chem. Soc. Rev.* **2019**, *48*, 4823−4853.

(15) Szilágyi, P. Á.; Lutz, M.; Gascon, J.; Juan-Alcañiz, J.; van Esch, J.; Kapteijn, F.; Geerlings, H.; Dam, B.; van de Krol, R. MOF@MOF Core-Shell vs. Janus Particles and the Effect of Strain: Potential for Guest Sorption, Separation and Sequestration. *CrystEngComm* **2013**, *15*, 6003−6008.

(16) Feng, L.; Wang, K. Y.; Willman, J.; Zhou, H. C. Hierarchy in Metal-Organic Frameworks. *ACS Cent. Sci.* **2020**, *6*, 359−367.

(17) Kim, R.; Ryu, U.; Jee, S.; Choi, K. M. Surface Coating of MOF Layers on the Nanocrystals of Other MOFs Using Nanoparticle Mediated Nucleation for the Efficient Removal of Formaldehyde. *Appl. Surf. Sci.* **2020**, *505*, No. 144612.

(18) Said, R. B.; Kolle, J. M.; Essalah, K.; Tangour, B.; Sayari, A. A Unified Approach to CO_2-Amine Reaction Mechanisms. *ACS Omega* **2020**, *5*, 26125−26133.

(19) Ye, J.; Kalvet, I.; Schoenebeck, F.; Rovis, T. Direct α-Alkylation of Primary Aliphatic Amines Enabled by CO_2 and Electrostatics. *Nat. Chem.* **2018**, *10*, 1037−1041.

(20) Dutcher, B.; Fan, M.; Russell, A. G. Amine-Based CO_2 Capture Technology Development from the Beginning of 2013−A Review. *ACS Appl. Mater. Interfaces* **2015**, *7*, 2137−2148.

(21) Flaig, R. W.; Osborn Popp, T. M.; Fracaroli, A. M.; Kapustin, E. A.; Kalmutzki, M. J.; Altamimi, R. M.; Fathieh, F.; Reimer, J. A.; Yaghi, O. M. The Chemistry of CO_2 Capture in an Amine-Functionalized Metal−Organic Framework under Dry and Humid Conditions. *J. Am. Chem. Soc.* **2017**, *139*, 12125−12128.

(22) Trickett, C. A.; Helal, A.; Al-Maythalony, B. A.; Yamani, Z. H.; Cordova, K. E.; Yaghi, O. M. The Chemistry of Metal-Organic Frameworks for CO_2 Capture, Regeneration and Conversion. *Nat. Rev. Mater.* **2017**, *2*, 17045.

(23) Ryu, U. J.; Kim, S. J.; Lim, H. K.; Kim, H.; Choi, K. M.; Kang, J. K. Synergistic Interaction of Re Complex and Amine Functionalized Multiple Ligands in Metal-Organic Frameworks for Conversion of Carbon Dioxide. *Sci. Rep.* **2017**, *7*, 612.

(24) Seo, H.; Rahimi, M.; Hatton, T. A. Electrochemical Carbon Dioxide Capture and Release with a Redox-Active Amine. *J. Am. Chem. Soc.* **2022**, *144*, 2164−2170.

(25) McDonald, T. M.; Lee, W. R.; Mason, J. A.; Wiers, B. M.; Hong, C. S.; Long, J. R. Capture of Carbon Dioxide from Air and Flue Gas in the Alkylamine-Appended Metal-Organic Framework mmen-Mg_2(dobpdc). *J. Am. Chem. Soc.* **2012**, *134*, 7056−7065.

(26) Hamdy, L. B.; Goel, C.; Rudd, J. A.; Barron, A. R.; Andreoli, E. The Application of Amine-Based Materials for Carbon Capture and Utilisation: An Overarching View. *Mater. Adv.* **2021**, *2*, 5843−5880.

(27) Qiao, Z.; Wang, N.; Jiang, J.; Zhou, J. Design of Amine-Functionalized MetalOrganic Frameworks for CO_2 Separation: The More Amine, the Better? *Chem. Commun.* **2016**, *52*, 974−977.

(28) Furukawa, H.; Gándara, F.; Zhang, Y. B.; Jiang, J.; Queen, W. L.; Hudson, M. R.; Yaghi, O. M. Water Adsorption in Porous Metal-Organic Frameworks and Related Materials. *J. Am. Chem. Soc.* **2014**, *136*, 4369−4381.

(29) Tang, X.; Luo, Y.; Zhang, Z.; Ding, W.; Liu, D.; Wang, J.; Guo, L.; Wen, M. Effects of Functional Groups of $-NH_2$ and $-NO_2$ on Water Adsorption Ability of Zr-Based MOFs (UiO-66). *Chem. Phys.* **2021**, *543*, No. 111093.

(30) KaiYue, S.; Da, Y.; HuaQiang, Y.; XueDong, H.; Tao, M.; Hua, F. Study on the Water Vapor Adsorption Characteristics of Carbon Materials in HTGR. *IOP Conf. Ser.: Mater. Sci. Eng.* **2021**, *1150*, No. 012008.

(31) Ko, N.; Hong, J.; Sung, S.; Cordova, K. E.; Park, H. J.; Yang, J. K.; Kim, J. Kim, A significant enhancement of water vapour uptake at low pressure by amine-functionalization of UiO-67. *Dalton Trans.* **2015**, *44*, 2047−2051.

(32) Boyde, A.; Mccorkell, F. A.; Taylor, G. K.; Bomphrey, R. J.; Doube, M. Iodine Vapor Staining for Atomic Number Contrast in Backscattered Electron and X-Ray Imaging. *Micros. Res. Tech.* **2014**, *77*, 1044−1051.

https://doi.org/10.1021/jacs.2c12207
J. Am. Chem. Soc. XXXX, XXX, XXX−XXX

(33) Yang, H.; Rutte, R. N.; Jones, L.; Simson, M.; Sagawa, R.; Ryll, H.; Huth, M.; Pennycook, T. J.; Green, M. L. H.; Soltau, H.; Kondo, Y.; Davis, B. G.; Nellist, P. D. Simultaneous Atomic-Resolution Electron Ptychography and Z-Contrast Imaging of Light and Heavy Elements in Complex Nanostructures. *Nat. Commun.* **2016**, *7*, 12532.
(34) Çakır, T. Determining the Photon Interaction Parameters of Iodine Compounds as Contrast Agents for Use in Radiology. *J. Radiat. Res. Appl. Sci.* **2020**, *13*, 252−259.
(35) De La Vega, J. C.; Esquinas, P. L.; Gill, J. K.; Jessa, S.; Gill, B.; Thakur, Y.; Saatchi, K.; Häfeli, U. O. Comparison of Rhenium and Iodine as Contrast Agents in X-Ray Imaging. *Contrast Media Mol. Imaging* **2021**, *2021*, 1−15.
(36) Lee, Y. R.; Do, X. H.; Cho, K. Y.; Jeong, K.; Baek, K. Y. Amine-Functionalized Zeolitic Imidazolate Framework-8 (ZIF-8) Nanocrystals for Adsorption of Radioactive Iodine. *ACS Appl. Nano Mater.* **2020**, *3*, 9852−9861.
(37) Falaise, C.; Volkringer, C.; Facqueur, J.; Bousquet, T.; Gasnot, L.; Loiseau, T. Capture of Iodine in Highly Stable Metal-Organic Frameworks: A Systematic Study. *Chem. Commun.* **2013**, *49*, 10320−10322.
(38) Zhang, X.; da Silva, I.; Fazzi, R.; Sheveleva, A. M.; Han, X.; Spencer, B. F.; Sapchenko, S. A.; Tuna, F.; McInnes, E. J. L.; Li, M.; Yang, S.; Schröder, M. Iodine Adsorption in a Redox-Active Metal−Organic Framework: Electrical Conductivity Induced by Host−Guest Charge-Transfer. *Inorg. Chem.* **2019**, *58*, 14145−14150.
(39) Wang, J.; Li, Z.; Wang, Y.; Wei, C.; Ai, K.; Lu, L. Hydrogen Bond-Mediated Strong Adsorbent-I_3^- Interactions Enable High-Efficiency Radioiodine Capture. *Mater. Horiz.* **2019**, *6*, 1517−1525.

https://doi.org/10.1021/jacs.2c12207
J. Am. Chem. Soc. XXXX, XXX, XXX−XXX